Theoretical temperature-electric-field phase diagram for betaine calcium chloride dihydrate

D. G. Sannikov* and G. Schaack
Physikalisches Institut der Universität Würzburg, Am Hubland, 97074 Würzburg, Federal Republic of Germany
(Received 22 January 1998; revised manuscript received 6 April 1998)

Theoretical phase diagrams for betaine calcium chloride dihydrate in the presence of an external electric field are calculated. A phenomenological approach applied earlier by the present authors [J. Phys.: Condens. Matter **10**, 1803 (1998)] for the construction of the temperature-pressure phase diagram, which is in agreement with the experimental diagram, is used. Expressions for thermodynamic potentials of different phases and for boundaries between these phases are given in an explicit or parametric form. The theoretical temperature-electric-field phase diagram is plotted and is compared with the experimental diagram.
[S0163-1829(98)00438-X]

I. INTRODUCTION

BCCD, $(CH_3)_3NCH_2COO\cdot CaCl_2\cdot 2H_2O$, is well known for its sequence of incommensurate (IC) and many commensurate ($C_{m/l}$) phases. The experimental temperature (T)-electric-field (E_y) phase diagram was determined recently at different values of pressure P from dielectric measurements.[1] It is shown schematically in Fig. 1 for $P=0$. The main specific feature of this diagram is that the regions of existence of commensurate phases, which have a spontaneous polarization P_y (along the field direction) increase as E_y grows. These $C_{m/l}$ phases with $P_y\neq 0$ are characterized by the dimensionless wave number $q=q_{m/l}=m/l=2/7, 2/9, 2/11, 0/1$; the $C_{0/1}$ phase is the low-temperature phase with $q=0$.

Several research groups have investigated the influence of E_y in BCCD and in partially and fully deuterated BCCD.[2–7] Dielectric[3,4,6] and pyroelectric[2,4] methods and elastic neutron scattering[5–7] were used and similar results for the extension of the polar $C_{m/l}$ phases were obtained. It was also observed that the field E_y can induce new $C_{m/l}$ phases with large l values. The experimental T-E phase diagram was constructed in Ref. 6 for the values 0, 2, and 4 kV cm^{-1} of the field E_y.

If the standard setting abc for the space group D_{2h}^{16} is used, then the space groups are $Pnma$ for the C phase and $Pn2_1a$ (C_{2v}^9) for the $C_{0/1}$ phase. The possible space groups of other $C_{m/l}$ phases are tabulated in Ref. 8. The wave vector of the IC phase is $k_z=qc^*$. Note, that for $E_y\neq 0$ the symmetry of the initial C and $C_{0/1}$ phases becomes identical, so that both phases merge into one C phase.

The main idea of the phenomenological approach as discussed in Ref. 8 is the following. Two different approaches for the description of the IC phase transitions are applied by us. One provides thermodynamic potentials for the C and IC phases, the other gives the potentials for the $C_{m/l}$ and the IC phases. Both approaches have to provide precisely the same expressions for the IC phase potential. Thus the thermodynamic potentials for all possible phases are obtained with self-consistent coefficients.

The aim of this paper is to construct theoretical phase diagrams for BCCD, starting from the phenomenological approach and considering the effect of an electric field E_y. First we construct the phase diagram in dimensionless coefficients D and A of thermodynamic potentials (see below). Assuming a linear dependence of D and A on T and P, we then construct the T-E phase diagram at $P=0$ and compare it with the experimental diagram[1] (Fig. 1).

II. THERMODYNAMIC POTENTIALS

Expressions for thermodynamic potentials of all possible phases in BCCD have been derived in Ref. 8. Here we use the same notations as in Ref. 8. The potential of the C and $C_{0/1}$ phases has the form

$$\Phi_C=\alpha P_y^2+\tfrac{2}{3}\beta P_y^4-P_yE_y, \tag{2.1}$$

where P_y is a homogeneous component of a polarization vector, provided the external field is assumed to be homogeneous, i.e., independent of z.

For the IC phase we use a single harmonic approximation:

$$P_y(z)=p+\sqrt{2}\rho\,\cos(qc^*z+\psi), \tag{2.2}$$

where the amplitude ρ, phase ψ, and wave number q are independent of z, while p is induced by the external field E_y. Then the potential of the IC phase has the form

$$\Phi_{IC}=\alpha(q)\rho^2+\beta\rho^4+\alpha p^2+\tfrac{2}{3}\beta p^4+4\beta\rho^2p^2-pE_y, \tag{2.3}$$

where

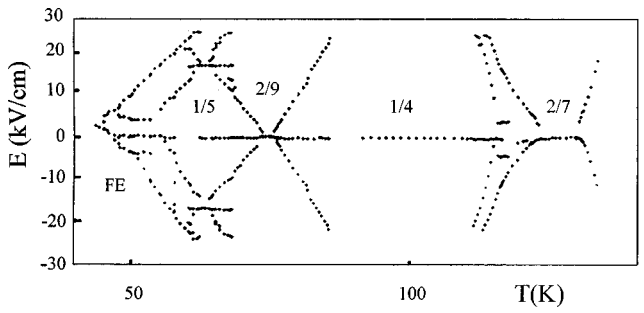

FIG. 1. Experimental T-E_y phase diagram for BCCD from Ref. 1.

$$\alpha(q)=\alpha-\delta q^2+\kappa q^4 \tag{2.4}$$

and it is necessary to assume $\beta>0, \kappa>0$, and also $\delta>0$.

The form of the potentials of the $C_{m/l}$ phases depends on the m/l value considered, i.e., whether m or l is even (+) or odd (−):

$$\Phi_{m_-/l_+}=\alpha(q_{m_-/l_+})R^2+\beta R^4-\tilde{\alpha}'_{2l}R^{2l}\cos 2l\varphi-b_5u_{zx}R^l\cos l\varphi+c_5u_{zx}^2-b_1P_xR^l\sin l\varphi+c_1P_x^2+\alpha P_y^2+\frac{2}{3}\beta P_y^4 +4\beta R^2P_y^2-P_yE_y, \tag{2.5}$$

$$\Phi_{m_-/l_-}=\alpha(q_{m_-/l_-})R^2+\beta R^4-\tilde{\alpha}'_{2l}R^{2l}\cos 2l\varphi-b_6u_{xy}R^l\sin l\varphi+c_6u_{xy}^2+\alpha P_y^2+\frac{2}{3}\beta P_y^4+4\beta R^2P_y^2-P_yE_y, \tag{2.6}$$

$$\Phi_{m_+/l_-}=\alpha(q_{m_+/l_-})R^2+\beta R^4-\tilde{\alpha}'_{2l}R^{2l}\cos 2l\varphi-b_2P_yR^l\cos l\varphi-b_4u_{yz}R^l\sin l\varphi+c_4u_{yz}^2+\alpha P_y^2+\frac{2}{3}\beta P_y^4+4\beta R^2P_y^2-P_yE_y. \tag{2.7}$$

Here R and φ are polar coordinates of a two-component order parameter. We assume that only one external force E_y is nonzero.

III. PARTIALLY MINIMIZED POTENTIALS

We now minimize the potentials given in the previous section with respect to those variables, for which the explicit expressions can be obtained, and thus partially simplify these potentials. Minimizing potential Eq. (2.3) with Eq. (2.4) of the IC phase with respect to q we obtain the equilibrium values of q:

$$q^2=\delta/2\kappa\equiv q_0^2, \quad \alpha_0\equiv\delta^2/4\kappa=\kappa q_0^4, \tag{3.1}$$

where the notation α_0 is introduced, which will be used in the following. Substituting Eq. (3.1) into Eqs. (2.3) and (2.4), we get

$$\alpha(q_0)=\alpha-\alpha_0. \tag{3.2}$$

Minimizing the potentials (2.5)–(2.7) of the $C_{m/l}$ phases with respect to the variables u_{zx} and P_x in Eq. (2.5), u_{xy} in Eq. (2.6), and u_{yz} in Eq. (2.7) we obtain

$$u_{zx}=(b_5/2c_5)R^l\cos l\varphi, \quad P_x=(b_1/2c_1)R^l\sin l\varphi, \quad u_{xy}=(b_6/2c_6)R^l\sin l\varphi, \quad u_{yz}=(b_4/2c_4)R^l\sin l\varphi. \tag{3.3}$$

Substituting Eq. (3.3) into Eqs. (2.5)–(2.7), we get

$$\Phi_{m_-/l_\pm}=\alpha(q_{m_-/l_\pm})R^2+\beta R^4-\alpha'_{2l}R^{2l}\cos 2l\varphi+\alpha P_y^2+\frac{2}{3}\beta P_y^4+4\beta R^2P_y^2-P_yE_y, \tag{3.4}$$

$$\Phi_{m_+/l_-}=\alpha(q_{m_+/l_-})R^2+\beta R^4-\alpha'_{2l}R^{2l}\cos 2l\varphi-b_2P_yR^l\cos l\varphi+\alpha P_y^2+\frac{2}{3}\beta P_y^4+4\beta R^2P_y^2-P_yE_y, \tag{3.5}$$

where

$$\alpha'_{2l}=\tilde{\alpha}'_{2l}+b_5^2/8c_5-b_1^2/8c_1, \quad \alpha'_{2l}=\tilde{\alpha}'_{2l}-b_6^2/8c_6, \quad \alpha'_{2l}=\tilde{\alpha}'_{2l}-b_4^2/8c_4 \tag{3.6}$$

for Φ_{m_-/l_+}, Φ_{m_-/l_-}, and Φ_{m_+/l_-}, respectively. The expressions for the potentials of the C_{m_-/l_+} and C_{m_-/l_-} phases are joined in one because of their similar form.

Minimizing the potentials (3.4) with respect to φ, we obtain for two possible phases c_1 and c_2 of each $C_{m/l}$ phase the solutions

$$\cos 2l\varphi=1, \quad \cos 2l\varphi=-1 \tag{3.7}$$

for c_1 and c_2, respectively. The phases c_1 and c_2 are stable at $\alpha'_{2l}>0$ and $\alpha'_{2l}<0$, respectively. Minimizing potential (3.5) with respect to φ, we obtain for phase c_1 the solution

$$\sin l\varphi=0, \quad \cos l\varphi=b_2/|b_2|. \tag{3.8}$$

At $E_y=0$ phase c_1 is stable at $\alpha'_{2l}>0$, so that we assume $\alpha'_{2l}>0$ to be valid in this case. The solution for phase c_2 is more complicated and we do not use it in the present context. The point is that all C_{m_+/l_-} phases that have been observed in experiment are polar ($P_y\neq 0$). This is established beyond doubt for the phases with $m/l=2/7, 2/9, 2/11, 2/13$ (see Ref. 1), and 4/15 (see Refs. 3 and 4) and is also evident for 6/23 (see Refs. 3 and 10). As a consequence, we shall only consider phase c_1 of the C_{m_+/l_-} phases.

By using Eqs. (3.7) and (3.8), solutions (3.3) for P_i and u_{ij} take the form

$$c_1:\ u_{zx}=\pm(b_5/2c_5)R^l, \quad P_x=0, \quad c_2:\ P_x=\pm(b_1/2c_1)R^l, \quad u_{zx}=0; \quad c_1:\ u_{xy}=0, \quad c_2:\ u_{xy}=\pm(b_6/2c_6)R^l; \quad c_1:\ u_{yz}=0 \tag{3.9}$$

for C_{m_-/l_+}, C_{m_-/l_-}, and C_{m_+/l_-} phases, respectively. The signs $\pm$ relate to different domains. In all cases $P_y \neq 0$ (see below). Substituting Eq. (3.7) into Eq. (3.4), and Eq. (3.8) into Eq. (3.5), we arrive at the expression

$$\Phi_{m/l} = \alpha(q_{m/l})R^2 + \beta R^4 - |\alpha'_{2l}|R^{2l} - |b_2|P_y R^l + \alpha P_y^2 + \frac{2}{3}\beta P_y^4 + 4\beta R^2 P_y^2 - P_y E_y, \tag{3.10}$$

where we join the potentials for all $C_{m/l}$ phases in one expression, thus lowering the number of expressions to be considered. We have to bear in mind that the coefficient $b_2 \neq 0$ only for C_{m_+/l_-} phases, while for C_{m_-/l_+} and C_{m_-/l_-} phases $b_2 = 0$.

IV. SET OF EQUATIONS

In the previous section we have partially simplified the expressions for the thermodynamic potentials: Eq. (2.1) of the $C = C_{0/1}$ phase, Eqs. (2.3) and (3.2) of the IC phase, and Eq. (3.10) of the $C_{m/l}$ phases. It is convenient to introduce dimensionless variables and coefficients which bring these potentials into the following form:

$$\phi_C = -(A - D^2)P_0^2 + \frac{2}{3}P_0^4 - P_0 E, \tag{4.1}$$

$$\phi_{IC} = -AR^2 + R^4 - (A - D^2)P^2 + \frac{2}{3}P^4 + 4R^2P^2 - PE, \tag{4.2}$$

$$\phi_{m/l} = -AR_l^2 + R_l^4 - (A - D^2)P_l^2 + \frac{2}{3}P_l^4 + 4R_l^2P_l^2 - P_l E + \{(D - q_{m/l}^2)^2 R_l^2 - (2A_l)^{l-1}R_l^{2l} - (2B_l)^{l/2-1}R_l^l P_l\}, \tag{4.3}$$

where

$$\Phi_{C,IC,m/l} = \phi_{C,IC,m/l}\Phi_0, \quad E_y = EE_0,$$
$$P_y, p, \rho, R, P_y = (P_0, P, R, R_l, P_l,)R_0, \tag{4.4}$$

$$\Phi_0 \equiv \frac{\kappa^2}{\beta}, \quad E_0^2 \equiv \frac{\kappa^3}{\beta}, \quad R_0^2 \equiv \frac{\kappa}{\beta}, \quad D \equiv \frac{\delta}{2\kappa}, \quad A \equiv \frac{\alpha_0 - \alpha}{\kappa},$$
$$A_l \equiv \frac{\kappa}{2\beta}\left(\frac{|\alpha'_{2l}|}{\kappa}\right)^{1/(l-1)}, \quad B_l \equiv \frac{\kappa}{2\beta}\left(\frac{b_2^2}{\kappa\beta}\right)^{1/(l-2)}.$$

for C, IC, and $C_{m/l}$ phases, respectively.

A somewhat different phenomenological approach for the description of the C, IC, $C_{m/l}$ phase transition sequence in an applied electric field E was used earlier in Ref. 6. The assumption $P_y(z) = R\cos qz$ is made by the authors of Ref. 6 when deriving potentials of the $C_{m/l}$ phases, which is not consistent with the requirement that the polarization has to be independent of the coordinates in the $C_{m/l}$ phases. Under such an assumption the improper polarization, the polarization induced by the external electric field E, and the interaction of these constant components of P with E are neglected. In addition, in Ref. 6, $|\alpha'_{2l}|R^{2l}$ and $|b_2|R^l$ have been approximated by $\alpha'_{eff}R^4$ and $b_{eff}R^4$, respectively. A constant P induced by E and the interaction energy of P with E have also been neglected when deriving the potential of the IC phase (see above). Moreover, besides the usual temperature dependence of α also the coefficient δ [Eq. (3.1)] depends on T but with an even stronger T dependence [see Fig. 2(a)], which has not been taken into account in Ref. 6.

Nevertheless, the theoretical T-E phase diagram constructed in Ref. 6 has some similarity with the T-E diagram as presented here in Fig. 3. Unfortunately, no information can be found in Ref. 6 on the construction of the diagram. If the phase sequence at $E = 0$ and the temperature intervals were taken from the experiment, then a specific choice of the potentials will only affect the form of the boundaries between neighboring phases. It is just the form of the phase boundaries that makes the difference between Fig. 12 in Ref. 6 and Fig. 3.

Minimizing now potentials (4.1), (4.2), and (4.3) with respect to the corresponding variables, we obtain the set of equations that determines equilibrium values of these variables:

$$\partial\phi_C/\partial P_0 = -2(A - D^2)P_0 + \frac{8}{3}P_0^3 - E = 0, \tag{4.5}$$

$$\partial\phi_{IC}/\partial P = -2(A - D^2)P + \frac{8}{3}P^3 + 8PR^2 - E = 0, \tag{4.6}$$

$$\partial\phi_{IC}/\partial R = 2R(-A + 2R^2 + 4P^2) = 0, \tag{4.7}$$

$$\partial\phi_{m/l}/\partial R_l = 2R_l\left[-A + 2R_l^2 + 4P_l^2 + \left\{(D - q_{m/l}^2)^2 - l(2A_lR_l^2)^{l-1} - \frac{l}{2}(2B_lR_l^2)^{l/2-1}P_l\right\}\right] = 0, \tag{4.8}$$

$$\partial\phi_{m/l}/\partial P_l = -2(A - D^2)P_l + \tfrac{8}{3}P_l^3 + 8P_lR_l^2 - E - \{(2B_lR_l^2)^{l/2-1}R_l^2\} = 0. \tag{4.9}$$

By solving this set of equations (4.5)–(4.8) together with the equations for the boundaries between different phases, we can construct the phase diagram in the D-A plane at fixed values of E and give values of the parameters A_l and B_l, while the value of $q_{m/l}$ is known in every case. Only one parameter A_l for m_-/l_+ and m_-/l_- and two parameters A_l and B_l for m_+/l_- describe each $C_{m/l}$ phase and have to be chosen in such a way as to provide the best agreement between theoretical and experimental phase diagrams.

V. C-IC BOUNDARY

We consider the set of equations (4.5)–(4.7) together with an equation for the boundary between C and IC phases:

$$\phi_C = \phi_{IC}, \tag{5.1}$$

where ϕ_C and ϕ_{IC} are taken from Eqs. (4.1) and (4.2).

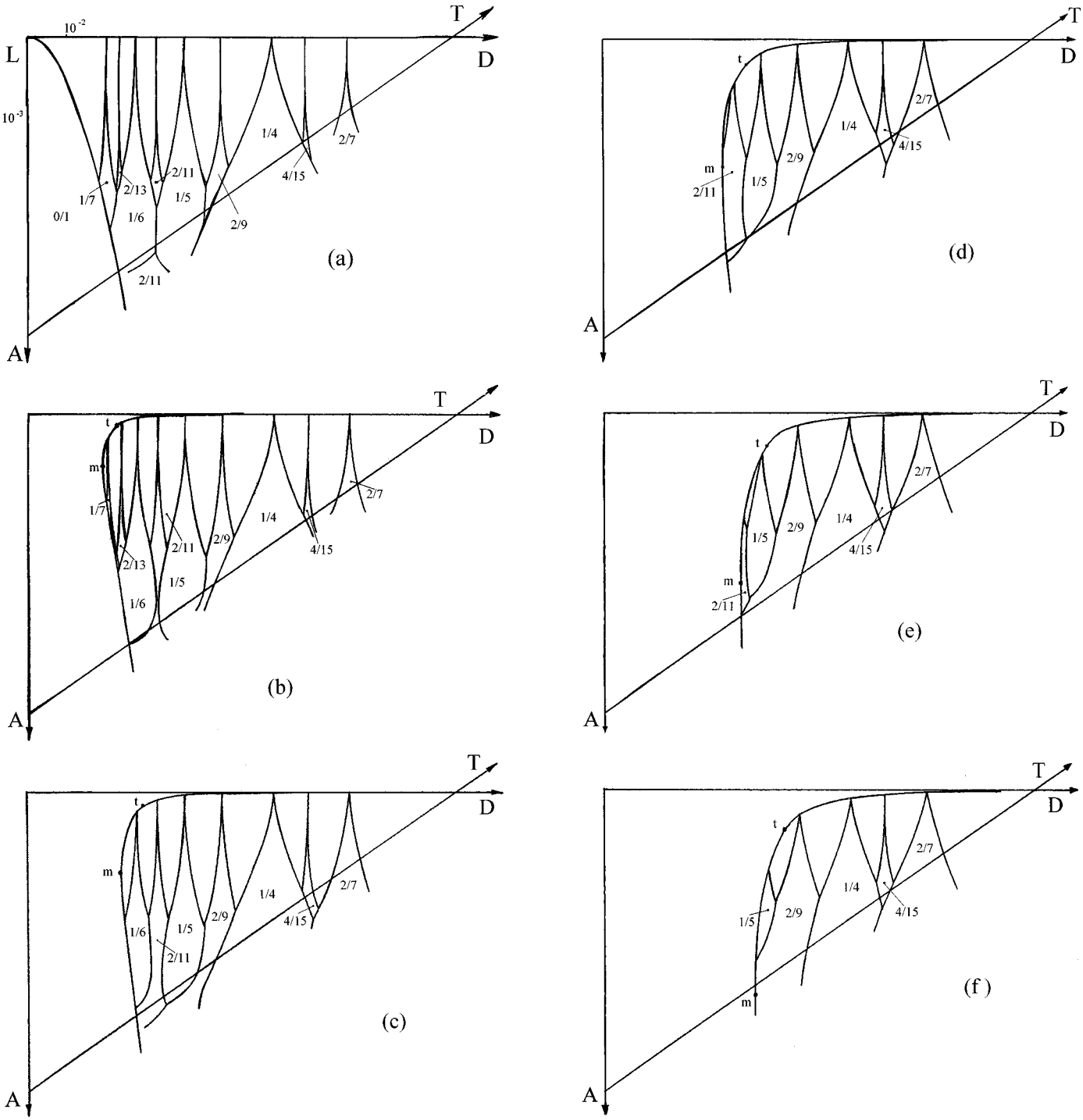

FIG. 2. *D-A* phase diagram for different values of E (in units of 10^{-6}). (a) $E=0$, (b) $E=5$, (c) $E=10$, (d) $E=20$, (e) $E=30$, (f) $E=40$, (g) $E=50$ (see text).

It follows from Eq. (4.7) that

$$R^2=A/2-2P^2. \tag{5.2}$$

From Eqs. (4.5) and (4.6), excluding R^2 according to Eq. (5.2), we obtain the expressions

$$A-D^2=\frac{4}{3}P_0^2-\frac{E}{2P_0}, \quad A+D^2=\frac{20}{3}P^2+\frac{E}{2P}, \tag{5.3}$$

which can be evidently resolved with respect to D^2 and A. Substituting Eqs. (5.2) and (5.3) into Eq. (5.1), we arrive at the equation

$$(24PP_0)^{-2}(P-P_0)^2[320P^2P_0^2(P+P_0)^2 + 48PP_0(5P-P_0)E-9E^2]=0. \tag{5.4}$$

We consider the first root $P=P_0$ of this equation. Substituting it into Eq. (5.3), we obtain the relation

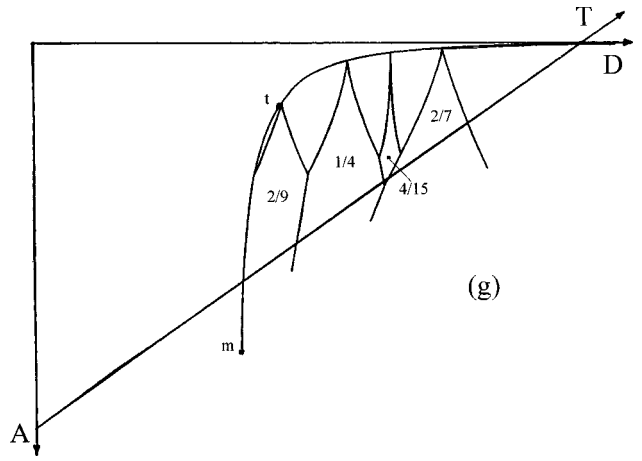

FIG. 2. (*Continued*).

$$D^2=\frac{2}{3}A+A^{-1/2}E. \tag{5.5}$$

This is the explicit expression for the C-IC boundary at constant $E\neq 0$. This boundary is a line of second-order phase transitions, since on this boundary $R=0$, which follows from Eqs. (5.2) and (5.3) at $P=P_0$. The line (5.5) asymptotically approaches the C-IC boundary $A=0$ at $E=0$ according to the relation $A=E^2/D^4$.

The line of second-order phase transitions, as determined by Eq. (5.5), terminates in the tricritical point (t point), where it changes to a line of first-order phase transitions. In order to find the coordinates of the t point, we substitute the root $P=P_0$ into the square brackets of Eq. (5.4). As a result we obtain by using Eq. (5.3)

$$A_t=(3E/10)^{2/3},\quad D_t^2=4A_t,\quad P_0^2=P^2=\tfrac{1}{4}A_t,\quad R=0, \tag{5.6}$$

where the values of P_0, P, and R in this point are also presented.

We also find the coordinates of the point at which the tangent to the C-IC boundary is parallel to the A axis in the D-A plane. We call it the m point. Taking the full derivative of Eq. (5.1) with respect to A, and using Eqs. (4.5)–(4.7) and the condition $dD/dA=0$, which determines the m point, we arrive at $P_0^2=R^2+P^2$. It follows from here and from Eqs. (5.2) and (5.4), that

$$A_m=\frac{25}{4}(3E/14)^{2/3},\quad D_m^2=\frac{14}{25}A_m, \tag{5.7}$$

$$P_0^2=\frac{49}{100}A_m,\quad P^2=\frac{1}{100}A_m,\quad R^2=\frac{12}{25}A_m,$$

where the values of P_0, P, and R in this point are also given.

The line of first-order phase transitions, unlike the line of second-order phase transitions, has a parametric representation: it is given by Eq. (5.4) in square brackets. In order to plot this line in the D-A plane at constant $E\neq 0$, we select a value of P and obtain the corresponding value of P_0 from Eq. (5.4). The values of D and A are then obtained from Eq. (5.3). The C-IC boundary plotted point by point and also by using formulas (5.5)–(5.7) is shown in Fig. 2. It is given for several values of the field E. It is also possible to obtain the explicit expression for the first-order C-IC phase transition line, which is asymptotically valid at large values of A and D, i.e., far from the m point in the form

$$A=cD^2-\sqrt{2(c-1)}E/D,\quad c\equiv(1-\sqrt{2/3})^{-1}\approx 5.45. \tag{5.8}$$

It can also be regarded as the expansion of a more precise expression in a power series in E with taking into account only the first term linear in E. The explicit expression for the C-IC boundary at $E=0$ follows from Eq. (5.8): $A=cD^2$. Evidently this can also be obtained from Eqs. (5.3) and (5.4).

VI. IC-$C_{m/l}$ BOUNDARIES

We consider the set of equations (4.6)–(4.9) together with an equation for the boundary between the IC and $C_{m/l}$ phases:

$$\phi_{IC}=\phi_{m/l}, \tag{6.1}$$

where ϕ_{IC} and $\phi_{m/l}$ are determined by Eqs. (4.2) and (4.3). Comparing potentials (4.2) and (4.3), it becomes evident that they differ by the terms in curly brackets. These terms are comparatively small (see below) and we use this fact to derive the IC-$C_{m/l}$ boundaries.

Solutions of Eqs. (4.6) and (4.7) for P and R can be obtained in the form of power series in the field E. Solutions of Eqs. (4.8) and (4.9) can be obtained assuming that the terms in curly brackets are small, and hence P_l-P and R_l-R are small quantities. Using these solutions we find from Eq. (6.1) the expression for the IC-$C_{m/l}$ boundary in the form

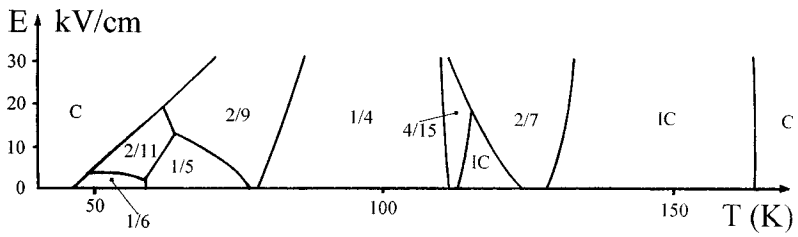

FIG. 3. Theoretical T-E phase diagram for BCCD.

$$(D-q_{m/l}^2)^2=\left[A_l\left(A-\frac{E^2}{(A+D^2)^2}\right)\right]^{l-1}+\left[B_l\left(A-\frac{E^2}{(A+D^2)^2}\right)\right]^{l/2-1}\frac{E}{2(A+D^2)}\times\left(1+\frac{5}{3}\frac{E^2}{(A+D^2)^3}\right)+(B_lA)^{l-2}\frac{A}{8(A+D^2)}. \tag{6.2}$$

The expressions in square brackets in Eq. (6.2) are not expanded in a power series in E to prevent the appearance of A in the denominators and thus to get the false impression that the expansion is invalid at small A values. In the last summand of Eq. (6.2) the bulky terms proportional to E^2 are dropped because they are not used here. In the first and second summand the terms proportional to E^2 are taken into account mainly in order to demonstrate the conditions at which Eq. (6.2) is valid.

The condition of weak anisotropy implies that the terms in the curly brackets are small as compared to the first term AR_l^2 in Eq. (4.3). In the case of $E=0$ the condition of weak anisotropy, as it follows from Eq. (6.2), has the form of two inequalities:

$$(A_lA)^{l-1}A^{-1}\ll 1, \quad (B_lA)^{l-2}[8(A+D^2)]^{-1}\ll 1. \tag{6.3}$$

The first of these inequalities is the condition of weak intrinsic anisotropy, caused by the smallness of the term $|\alpha_{2l}'|R^{2l}$ with respect to the term $\alpha(q_{m/l})R^2$ in Eq. (3.10). The second inequality in Eq. (6.3) is connected with the term $|b_2|P_yR^l$ in potential (3.10). The role of this term manifests itself twice: P_y consists of the spontaneous (improper) polarization P_s and the polarization P_E induced by the field E. If P_s is eliminated from the potential at $E=0$, the coefficient α_{2l}' is renormalized, i.e., the term $b_2^2/8(\alpha+4\beta R^2)$ is added to it. This additional term must be also comparatively small, as is just expressed by the second inequality in Eq. (6.3). [Compare with the argument in Ref. 8, where the second inequality in Eq. (6.3) was not considered, since the coefficient b_2 has no independent meaning at $E=0$ and the renormalized coefficient α_{2l}' was considered as an entity without dividing it into parts.]

P_E and hence the term $|b_2|P_ER^l$ in potential (3.10) is induced by the field E. This term has to be small as compared to the term $\alpha(q_{m/l})R^2$ in Eq. (3.10). This condition is determined by the first inequality in

$$(B_lA)^{l/2-1}A^{-1}(A+D^2)^{-1}E\ll 1, \quad E^2(A+D^2)^{-3}\ll 1. \tag{6.4}$$

Here B_l occurs in a combination with E, which is the reason to give the second inequality separately in Eq. (6.3). The second inequality in Eq. (6.4), which restricts the value of E, is the condition of the validity of the expansion of P and R in powers of E (see above). The expansion is in fact performed in terms of the quantity on the left side of the inequality.

It follows from Eq. (6.2) that the boundaries between the IC phase and the C_{m_-/l_+} and C_{m_-/l_-} phases ($B_l=0$) are shifted by the field E insignificantly, proportionally to E^2. The shift of the boundaries between the IC phase and the C_{m_+/l_-} phases ($B_l\neq 0$) is proportional to E and depends also on the value of the coefficient B_l. This shift occurs to the side of the IC phase so that the area of existence of the C_{m_+/l_-} phases increases with E.

The four inequalities (6.3) and (6.4) determine the range of validity of formula (6.2). Actually, when plotting the boundary in the D-A phase diagram, we can use the simplified expression for the IC-$C_{m/l}$ boundaries, where the terms proportional to E^2 are omitted:

$$(D-q_{m/l}^2)^2=(A_lA)^{l-1}+\frac{1}{8}(B_lA)^{l-2}\frac{A}{A+D^2}+\frac{1}{2}(B_lA)^{l/2-1}\frac{E}{A+D^2}. \tag{6.5}$$

Note that the denominator in $E/(A+D^2)$ is a small quantity that amplifies the influence of the field E_y as compared to other external forces [see Eqs. (2.5)–(2.7)].

The IC-$C_{m/l}$ boundaries plotted by using formula (6.5) are shown in Fig. 2. The same E values have been used as for the plot of the C-IC boundary. The choice of the parameters A_l for the $C_{m/l}$ phases and of B_l for the C_{m_+/l_-} phases is discussed in Sec. IX.

VII. $C_{m/l}$-$C_{m'/l'}$ BOUNDARIES

We consider the set of equations (4.8) and (4.9) together with the equation for the boundaries between different $C_{m/l}$ and $C_{m'/l'}$ phases:

$$\phi_{m/l}=\phi_{m'/l'}, \tag{7.1}$$

where $\phi_{m/l}$ and $\phi_{m'/l'}$ are taken from Eq. (4.3). Using the same method and under the same approximations as in the previous section, when the inequalities (6.3) and (6.4) are valid, we obtain the expression for the $C_{m/l}$-$C_{m'/l'}$ boundaries in the form

$$D=\frac{1}{2}(q_{m/l}^2+q_{m'/l'}^2)-\frac{1}{2}(q_{m/l}^2+q_{m'/l'}^2)^{-1}\left(\left[A_l\left(A-\frac{E^2}{(A+D^2)^2}\right)\right]^{l-1}-\left[A_{l'}\left(A-\frac{E^2}{(A+D^2)^2}\right)\right]^{l'-1}+\left\{\left[B_l\left(A-\frac{E^2}{(A+D^2)^2}\right)\right]^{l/2-1}-\left[B_{l'}\left(A-\frac{E^2}{(A+D^2)^2}\right)\right]^{l'/2-1}\right\}\frac{E}{2(A+D^2)}\left(1+\frac{5}{3}\frac{E^2}{(A+D^2)^3}\right)+[(B_lA)^{l-2}-(B_{l'}A)^{l'-2}]\frac{A}{8(A+D^2)}\right). \tag{7.2}$$

When plotting the boundaries in the D-A phase diagram, we can actually use the simplified expression

$$D=\tfrac{1}{2}(q_{m/l}^2+q_{m'/l'}^2)-\frac{1}{2}(q_{m/l}^2-q_{m'/l'}^2)^{-1}$$
$$\times\{(A_lA)^{l-1}-(A_{l'}A)^{l'-1}+\tfrac{1}{2}[(B_lA)^{l/2-1}-(B_{l'}A)^{l'/2-1}]E(A+D^2)^{-1}+\tfrac{1}{8}[(B_lA)^{l-2}-(B_{l'}A)^{l'-2}]A(A+D^2)^{-1}\} \tag{7.3}$$

instead of Eq. (7.2), where terms proportional to E^2 are neglected, as was done in Eq. (6.5) in comparison with Eq. (6.2). Note that the boundaries IC-$C_{m/l}$, IC-$C_{m'/l'}$ [Eq. (6.5)], and $C_{m/l}$-$C_{m'/l'}$ [Eq. (7.3)] intersect at a single point, as they should. The same is valid for the boundaries $C_{m'/l'}$-$C_{m/l}$, $C_{m/l}$-$C_{m''/l''}$, and $C_{m'/l'}$-$C_{m''/l''}$ as well. The boundaries between different $C_{m/l}$ phases, plotted according to Eq. (7.3), are given in Fig. 2. The choice of the coefficients $A_l, B_l, A_{l'}, B_{l'}$ is discussed below in Sec. IX.

In the following, some notes about the C-$C_{m/l}$ boundaries are made. At $E=0$ each $C_{m/l}$ phase borders the C phase at a point with the coordinates $A=0, D=q_{m/l}^2$. It can border the $C_{0/1}$ phase along a line that usually differs insignificantly from the $C_{0/1}$-IC boundary.

At $E\neq 0$ and at small values of A the $C_{m/l}$ phase borders the C phase also at one point (the same as for $E=0$). This point lies on the line of second-order phase transitions C-IC. Its coordinates are $D=q_{m/l}^2$ and A is determined by Eq. (5.5). This is valid for values of E that satisfy $D_t<q_{m/l}^2$ [see Eq. (5.6)], i.e., if the point is on the right of the t point. At higher fields E, when $q_{m/l}^2<D_t$, the $C_{m/l}$ phase borders the C phase along a line that is the shorter the nearer it lies to the t point.

At large values of $A(E\neq 0)$ the $C_{m/l}$ phase borders the C phase also along a line. At higher values of the field E the two boundaries of the $C_{m/l}$ phase with the C phase (at small A and at large A) can merge into a single boundary including the m point. Consequently, the $C_{m/l}$ phase borders the IC phase at the right and the C phase at the left side. At still higher values of the field the $C_{m/l}$ phase disappears due to the shift of the C-IC boundary toward the right with increasing E (see Fig. 2).

We suppose that the C-$C_{m/l}$ boundary does not significantly differ from the C-IC boundary and when constructing the D-A diagram we neglected this difference. Therefore we do not derive expressions for the C-$C_{m/l}$ boundaries here.

VIII. ESTIMATE OF COEFFICIENTS OF THERMODYNAMIC POTENTIALS

In order to construct the T-E phase diagram from the D-A diagram it is necessary to have information on the magnitude of some coefficients of the thermodynamic potentials. They can be estimated by a comparison of the theoretical and the experimental T-E phase diagrams, since the latter contains a large amount of information. It is also possible for the evaluation of the coefficients to use additional experimental data. We begin by following this second path and give some formulas.

Two coefficients of the thermodynamic potential are anomalously small: these are α and δ, see (2.4), since α vanishes at the Curie point $T=\Theta$, while δ determines the square of the equilibrium wave number [see Eq. (3.1)], which is also small. Hence the dependence of these coefficients on T and P is essential (see also Ref. 9). The other coefficients $\kappa, \beta, \alpha_{2l}', b_2$ have in general normal magnitudes. It is therefore possible to neglect their dependence on T and P, regarding them as constants. The dependence of δ and α on T and P is supposed to be linear:

$$\begin{aligned}\delta(T,P)&=\delta_i+\delta_T(T-T_i)-\delta_P P,\\ \alpha(T,P)&=\alpha_i+\alpha_T(T-T_i)-\alpha_P P,\\ \alpha_i&=\alpha_T(T_i-\Theta),\end{aligned} \tag{8.1}$$

where Θ is the Curie temperature at $P=0$ and T_i is the temperature of the C-IC phase transition at $P=0$.

It follows from Eq. (8.1) and from Eqs. (3.1) and (3.2), that

$$\begin{aligned}q_i^2\equiv q_0^2|_{T=T_i,P=0}&=\frac{\delta_i}{2\kappa},\\ \alpha_i\equiv\alpha_0|_{T=T_i,P=0}&=\frac{\delta_i^2}{4\kappa}=\kappa q_i^4.\end{aligned} \tag{8.2}$$

From Eqs. (8.1) and (3.1) we find

$$q_{m/l}^2=q_i^2-\frac{\delta_T}{2\kappa}(T_i-T_{m/l}), \tag{8.3}$$

where $T_{m/l}$ is an average temperature of the $C_{m/l}$ phase under the condition, that this phase exists in a narrow temperature interval. It also follows from Eqs. (8.1) and (3.1), that

$$\frac{\partial}{\partial T}q_0^2\bigg|_{T=T_i,P=0}=\frac{\delta_T}{2\kappa},\quad \frac{\partial}{\partial P}q_0^2\bigg|_{T=T_i,P=0}=-\frac{\delta_P}{2\kappa}. \tag{8.4}$$

For the dielectric permittivity $\chi=dP_y/dE_y$ in the C phase and for the spontaneous polarization P_s in the $C_{0/1}$ phase at $E_y=0$, we obtain from Eq. (2.1) the expressions

$$\begin{aligned}&\chi^{-1}=2\alpha,\quad \chi^{-1}|_{P=0}=2\alpha_T(T-\Theta),\quad P_s^2=3(-\alpha)/4\beta,\\ &P_s^2|_{T=T_C,P=0}=3\alpha_T(\Theta-T_C)/4\beta,\end{aligned} \tag{8.5}$$

where T_c is the temperature of the transition into the $C_{0/1}$ phase.

For the jump of the specific heat $\Delta C=-T\partial^2\Phi_{IC}/\partial T^2|_{T=T_i,P=0}$ at $E_y=0$ we obtain from Eq. (2.3) and, by taking Eq. (3.2) into account, the expression

$$\Delta C=(T_i/2\beta)(\alpha_T-q_i^2\delta_T)^2. \tag{8.6}$$

Taking the total derivative with respect to P of the equation $\alpha=\alpha_0$, which is valid at $T\equiv T_i(P)$, we obtain as the result

$$\left.\frac{dT_i(P)}{dP}\right|_{P=0}=\frac{\alpha_P-q_i^2\delta_P}{\alpha_T-q_i^2\delta_T}. \tag{8.7}$$

Now we make use of experimental data. Some values, which have been given in many papers, are

$$T_i=164\ \text{K},\quad T_c=46\ \text{K},\quad q_i=0.32,$$
$$\rho=1.46\ \text{g cm}^{-3},\quad M=264.2\ \text{g mol}^{-1}, \tag{8.8}$$

where ρ is the density, M is the molecular weight of BCCD.

Using formula (8.2) for q_i^2 and the value of q_i [Eq. (8.8)], we obtain an estimate

$$q_i^2=\delta_i/2\kappa=0.10. \tag{8.9}$$

Using formula (8.4) we find from the temperature dependence of $q_0(T)$ given in Ref. 10 the estimate

$$\delta_T/2\kappa=7\times10^{-4}\ \text{K}^{-1}. \tag{8.10}$$

The magnitude of $\delta_T/2\kappa$ can be estimated also by using formula (8.3) for $q_{m/l}=2/7$, the average value of $T_{2/7}=126$ K (Refs. 10 and 11), the value of T_i [Eq. (8.8)], and the value $q_i=0.33$, which follows from the diagram of $q_0(T)$ given in Ref. 10. We obtain the same estimate as in Eq. (8.10).

Data of the dielectric constant are given in Ref. 12:

$$\epsilon_b(T)-\epsilon_\infty=C/(T-T_0),\quad C=1400\ \text{K},\quad T_0=130\ \text{K}. \tag{8.11}$$

Using formula (8.5) for χ we get from Eq. (8.11)

$$\alpha_T=2\pi/C=4.5\times10^{-3}\ \text{K}^{-1},\quad \Theta=T_0=130\ \text{K}. \tag{8.12}$$

Using formula (8.1) for α_i, and values from Eq. (8.8) of T_i, together with values of α_T and Θ from Eq. (8.12), we obtain

$$\alpha_i=0.15. \tag{8.13}$$

We now have to find estimates for κ and β, which are very important since they determine the value of E_0 [see Eq. (4.4)]. Using formula (8.2) for α_i, the values (8.8) of q_i and (8.13) of α_i, we find

$$\kappa=15. \tag{8.14}$$

For the jump of the specific heat the value

$$\Delta C_P=12.0\ \text{J mol}^{-1}\ \text{K}^{-1}=0.66\times10^6\ \text{dyn cm}^{-2}\ \text{K}^{-1} \tag{8.15}$$

is given in Ref. 13. The last value of ΔC_P is obtained by using values [Eq. (8.8)] of ρ and M. Using formula (8.6), values of T_i and q_i [Eq. (8.8)], of $\delta_T/2\kappa$ [Eq. (8.10)], of α_T [Eq. (8.12)], and of κ [Eq. (8.14)], we arrive at

$$\beta=7\times10^{-10}\ \text{dyn}^{-1}\ \text{cm}^2=8\times10^{-9}\ \text{cm}^2\ \text{kV}^{-2}. \tag{8.16}$$

Another estimate of β can be obtained by using formula (8.5) for P_s. Different values of P_s are found in the literature:

$$P_s=2.1,\ 2.3,\ 2.4\ \mu\text{C cm}^{-2}, \tag{8.17}$$

respectively, in Refs. 1, 14, and 15. Taking values of T_c [Eq. (8.8)], of Θ and α_T [Eq. (8.12)], we find the estimate

$$\beta=8\times10^{-8},\quad 7\times10^{-8},\quad 6\times10^{-8}\ \text{cm}^2\ \text{kV}^{-2}, \tag{8.18}$$

which are markedly inconsistent with Eq. (8.16).

For E_0 [see Eq. (4.4)], using values of κ [Eq. (8.14)] and of β [Eq. (8.16) or Eq. (8.18)], we obtain, respectively,

$$E_0=7\times10^5,\quad 2\times10^5\ \text{kV cm}^{-1}. \tag{8.19}$$

Unfortunately no experimental data on the dependence of q_0 on P near $T=T_i$ are known. Therefore no estimate of $\delta_P/2\kappa$ using Eq. (8.4) is possible. We might try to use Eq. (8.7). The values

$$\left.\frac{dT_i}{dP}\right|_{P=0}=0.177,\quad 0.176\ \text{K MPa}^{-1} \tag{8.20}$$

are given in tables in Refs. 16–18. However, as the estimates given below will show, the terms in the numerator and denominator of Eq. (8.7) are close in magnitude and hence will cancel. Therefore we cannot use Eqs. (8.7) and (8.20) for estimates of the coefficients.

Now we consider the theoretical phase diagram constructed in Ref. 8, which gives good chances for estimates of the coefficients. Using Eqs. (4.4), (8.1), (3.1), and (8.2) we obtain

$$D=q_i^2-\frac{\delta_T}{2\kappa}(T_i-T)-\frac{\delta_P}{2\kappa}P,$$
$$A=\left(\frac{\alpha_T}{\kappa}-2q_i^2\frac{\delta_T}{2\kappa}\right)(T_i-T)+\left(\frac{\alpha_P}{\kappa}-2q_i^2\frac{\delta_P}{2\kappa}\right)P. \tag{8.21}$$

The coordinates of the i point ($T=T_i$, $P=0$) on the D-A diagram were chosen in agreement with the value $q_i=0.33$ [Ref. 10, compare with Eq. (8.8)]. The D and A coordinates of the c point ($T=T_C$, $P=0$) allow us by using Eq. (8.21) to obtain the estimates

$$\delta_T/2\kappa=7\times10^{-4}\ \text{K}^{-1},\quad \alpha_T/\kappa=2\times10^{-4}\ \text{K}^{-1}, \tag{8.22}$$

where the first estimate agrees with Eq. (8.10). From Eq. (8.22) and from the value of α_T [Eq. (8.12)] we obtain [compare with Eq. (8.14)]:

$$\kappa=25. \tag{8.23}$$

The coordinates of the d point in the experimental T-P diagram are $T=T_i$, $P=P_d=360$ MPa.[1] The D and A coordinates of the d point in the D-A phase diagram[8] allow the following estimates by using Eq. (8.21):

$$\delta_P/2\kappa = 3\times 10^{-4}\ \mathrm{MPa}^{-1}, \quad \alpha_P/\kappa = 6\times 10^{-5}\ \mathrm{MPa}^{-1}. \tag{8.24}$$

Finally, from a comparison of the slope of the C phase boundary near $T=T_C$ in the experimental (Fig. 1) and the theoretical phase diagrams (Fig. 3) the estimate

$$E_0 = 6\times 10^5\ \mathrm{kV\ cm}^{-1} \tag{8.25}$$

can be derived [compare with the estimates of Eq. (8.19)]. For the construction of the T-E diagram in Fig. 3 the value of Eq. (8.25) is used.[19]

IX. THEORETICAL D-A AND T-E PHASE DIAGRAMS

We now proceed to the discussion of Fig. 2, where a sequence of fields E was chosen for the presentation. The selected values of the field $E=(0,5,10,20,30,40,50)\times 10^{-6}$ according to Eqs. (4.4) and (8.25) correspond to values of the field $E_y=(0,3,6,12,18,24,30)\times 10^3$ V/cm. On constructing the boundaries we have chosen the following values of constants:

$$A_4=30, \quad A_5=40, \quad A_6=60, \quad A_7=70, \tag{9.1}$$

respectively, for $l/m=1/4$, 1/5, 1/6, and 1/7, and

$$B_7=180, \quad A_7=0, \quad B_9=160, \quad A_9=0, \quad B_{11}=170, \quad A_{11}=0, \quad B_{15}=320, \quad A_{15}=0, \tag{9.2}$$

respectively, for $l/m=2/7$, 2/9, 2/11, and 4/15. These values have been determined to obtain an optimum agreement between experimental and theoretical T-E phase diagrams. Note that the values in Eq. (9.1) are correct up to the first digit, the values in Eq. (9.2) up to the second digit, while the values $A_{7,9,11,15}$ are taken equal to zero, since a selection of specific values ($\neq 0$) of these coefficients would exceed the accuracy of the experiment.[1]

The position and inclination of the T axis in Fig. 2 are also chosen for a good agreement with the experimental data [$\tan(\widehat{TD})=0.035$, see also Ref. 8, where $\tan(\widehat{TD})=0.038$].

We have transferred points of intersection between phase boundaries and the T axis at different values of E_y from Fig. 2 to construct Fig. 3. Figure 3 is plotted at the same scale as Fig. 1 for convenience of comparison. Note that in Fig. 1, unlike Fig. 3, the boundaries between nonpolar phases (C-IC, $C_{1/5}$-$C_{1/6}$) do not exist, because they cannot be measured by dielectric methods. The most essential difference between Figs. 1 and 3 is a triple point in Fig. 3, where three phases $C_{1/5}$, $C_{2/9}$, and $C_{2/11}$ meet, while in Fig. 1 one more phase, the nature of which is not established (see, however, Ref. 1 for a discussion), borders at the same point. In general, however, the agreement with the experimental T-E phase diagram appears acceptable.

In conclusion, we enumerate again all approximations and assumptions made, when constructing the theoretical D-A and T-P phase diagrams. Only two coefficients of thermodynamic potentials were assumed to depend linearly on temperature; all other coefficients were considered as constant.

The single-harmonic approximation was used for the IC phase (more exactly, the zeroth and the first harmonics were considered). If at least the second harmonic were taken into account, the results can be improved, especially at higher field strengths E.

The weak-anisotropy condition was used for the $C_{m/l}$ phases; both the intrinsic anisotropy and the anisotropy induced by the external electric field were assumed to be weak. This condition is the better fulfilled, the smaller are the constants A_l, B_l, and $1/l$ and the variables A and E. In Figs. 2 and 3 this condition is fairly well fulfilled.

The distinction between the C-IC and $C_{m/l}$-C boundaries was not taken into account. However, this distinction can be important and should be considered in a more elaborate approach. More precise values of the constants A_l and B_l and also of the slope of the T axis with respect to the D axis should improve the agreement and may be the object of future research.

Despite all of these approximations and assumptions we succeeded in calculating the theoretical T-E phase diagram in fairly good agreement with the experimental data. The phenomenological approach used in this paper to construct the T-E phase diagram and the T-P diagram in Ref. 8 has a larger range of validity than demonstrated here for BCCD. It can be applied to any crystal with a Lifshitz point in the phase diagram, e.g., to thiourea.

ACKNOWLEDGMENT

One of the authors (D.G.S.) gratefully acknowledges the financial support by the Deutsche Forschungsgemeinschaft.

*Permanent address: Shubnikov Institute of Crystallography, Russian Academy of Sciences, Moscow 117333, Russia.

[1] G. Schaack, M. le Maire, M. Schmitt-Lewen, M. Illing, A. Lengel, M. Manger, and R. Straub, Ferroelectrics **183**, 205 (1996); M. le Maire, R. Straub, and G. Schaack, Phys. Rev. B **56**, 134 (1997).

[2] J. L. Ribeiro, M. R. Chaves, A. Almeida, J. Albers, A. Klöpperpieper, and H. E. Müser, Phys. Rev. B **39**, 12 320 (1989).

[3] O. Freitag and H.-G. Unruh, Ferroelectrics **105**, 357 (1990).

[4] J. L. Ribeiro, M. R. Chaves, A. Almeida, H. E. Müser, J. Albers, and A. Klöpperpieper, Ferroelectrics **105**, 363 (1990).

[5] M. R. Chaves, A. Almeida, J. M. Kiat, W. Schwarz, J. Schneck, J. C. Tolédano, A. Klöpperpieper, H. E. Müser, and J. Albers, Phys. Rev. B **46**, 3098 (1992).

[6] M. R. Chaves, A. Almeida, J. C. Tolédano, J. Schneck, J. M. Kiat, W. Schwarz, J. L. Ribeiro, A. Klöpperpieper, J. Albers, and H. E. Müser, Phys. Rev. B **48**, 13 318 (1993).

[7] O. Hernandez, J. Hlinka, and M. Quilichini, Ferroelectrics **185**, 213 (1996).

[8] D. G. Sannikov and G. Schaack, J. Phys.: Condens. Matter **10**, 1803 (1998).

[9] V. A. Golovko, J. Phys.: Condens. Matter **2**, 5679 (1990).

[10] H.-G. Unruh, F. Hero, and V. Dvořák, Solid State Commun. **70**, 403 (1989).

[11] R. Ao, G. Schaack, M. Schmitt, and M. Zöller, Phys. Rev. Lett. **62**, 183 (1989).

[12] H. Wilhelm and H.-G. Unruh, Z. Kristallogr. **195**, 75 (1991).

[13] W. Brill, E. Gmelin, and K. H. Ehses, Ferroelectrics **103**, 25 (1990).

[14] A. Klöpperpieper, H. J. Rother, J. Albers, and H. E. Müser, Jpn. J. Appl. Phys., Suppl. **24-2**, 829 (1985).
[15] H. J. Rother, J. Albers, and A. Klöpperpieper, Ferroelectrics **54**, 107 (1984).
[16] G. Schaack, Ferroelectrics **104**, 147 (1990).
[17] G. Schaack, Acta Phys. Pol. A **83**, 451 (1993).
[18] G. Schaack and M. le Maire, Ferroelectrics **208**, 1 (1998).
[19] It is necessary to emphasize that most of the estimates of coefficients obtained in this section are correct at best up to the order of magnitude.